Enrichment of Paramagnetic Ions from Homogeneous Solutions in Inhomogeneous Magnetic Fields

ARTICLE *in* JOURNAL OF PHYSICAL CHEMISTRY LETTERS · DECEMBER 2012

Impact Factor: 7.46 · DOI: 10.1021/jz301561q

THE JOURNAL OF PHYSICAL CHEMISTRY Letters

Letter

pubs.acs.org/JPCL

Enrichment of Paramagnetic Ions from Homogeneous Solutions in Inhomogeneous Magnetic Fields

Xuegeng Yang,*[,†] Kristina Tschulik,[‡] Margitta Uhlemann,[‡] Stefan Odenbach,[†] and Kerstin Eckert*[,†]

[†]Institute of Fluid Mechanics, Chair of Magnetofluiddynamics, Technische Universität Dresden, D-01069 Dresden, Germany

[‡]IFW Dresden, P.O. Box 270016, D-01171 Dresden, Germany

Supporting Information

ABSTRACT: Applying interferometry to an aqueous solution of paramagnetic manganese ions, subjected to an inhomogeneous magnetic field, we observe an unexpected but highly reproducible change in the refractive index. This change occurs in the top layer of the solution, closest to the magnet. The shape of the layer is in accord with the spatial distribution of the largest component of the magnetic field gradient force. It turns out that this layer is heavier than the underlying solution because it undergoes a Rayleigh−Taylor instability upon removal of the magnet. The very good agreement between the magnitudes of buoyancy, associated with this layer, and the field gradient force at steady state provides conclusive evidence that the layer formation results from an enrichment of paramagnetic manganese ions in regions of high magnetic field gradient.

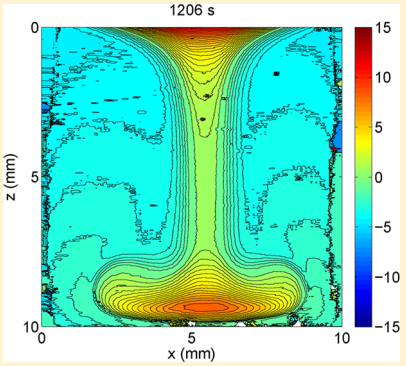

SECTION: Liquids; Chemical and Dynamical Processes in Solution

Magnetic field is a powerful tool to create flows on vastly different length scales in a noninvasive way.[1−3] Time-dependent magnetic fields, applied to liquid metals, are able to stir and homogenize melts,[1,4] in this way governing the microstructural evolution of casting alloys.[5] Static fields, applied to electrolytes, considerably improve the quality of electrodeposits[6] or can be used for magnetohydrodynamic pumping, for example, for lab-on-a-chip devices.[7,8] For these applications, the Lorentz force density, $\vec{f}_L = \vec{j} \times \vec{B}$, given by the cross product of the electric current density $\vec{j}$ and magnetic induction $\vec{B}$, is utilized, which homogeneously acts on the entire fluid.[1]

However, an increasing interest is noticeable in the application of magnetic fields to manipulate objects according to their magnetic properties, both on the macroscale, for example, in sorting scrap metal, and on the microscale, mostly related to biomedical applications.[9−11] One focus, for example, is on the application of magnetophoresis to separate functionalized magnetic particles[10,12] and to open avenues for studying living cells.[13] These applications are based on the magnetic field gradient force density[14]

$$\vec{f}_m = \frac{\chi_{sol}}{\mu_0}(\vec{B}\cdot\nabla)\vec{B} \tag{1}$$

which depends on the magnetic susceptibility χ_{sol} of the medium or object concerned and on the magnetic field gradients applied; $\mu_0 = 4\pi \times 10^{-7}$ V s/(A m) denotes the vacuum permeability.

Although high gradients of more than 10^3 T/m may be generated easily,[15] it has been reported that this force can only be used to manipulate macro-, micro-, and nanoscale particles. However, even controlling of superparamagnetic nanoparticles in field gradients is a formidable task because the processes involved scale differently with respect to the particle size. The theory of Brownian motion shows that the smaller the particle size, the larger the mean-squared displacement. This makes it difficult for the field gradient force, scaling with the cube of the particle diameter, to track such small particles at all. Thus, with a view to the atomic scale, corresponding to paramagnetic ions or molecules, it is considered even less likely that $\vec{f}_m$ will have any impact due to the tremendous difference of about five orders in magnitude between the kinetic energy of $3/2kT$ at temperature T, associated with the Brownian motion (k, Boltzmann constant), and the magnetic energy, proportional to the magnetic moment of the molecule times $\vec{B}$. In accordance with this belief, some authors[16] have claimed that a magnetic-field gradient-based manipulation of fluids is only possible for nonhomogeneous liquid media, yet it has been reported that because of thermal diffusion homogeneous mixtures are eventually obtained in all cases and that magnetic gradient fields are not observed to have an effect on homogeneous systems, for example, solutions of paramagnetic ions.[16] In another approach,[17,18] the drift motion of paramagnetic metal ions is studied after a small volume of metal ion solution has been spotted on silica gel and exposed to an inhomogeneous magnetic field. They conclude that metal ions do not move as

Received: October 2, 2012
Accepted: November 14, 2012

   dx.doi.org/10.1021/jz301561q | J. Phys. Chem. Lett. 2012, 3, 3559−3564

single ions but as a group of ions and water molecules with an estimated diameter of 2.4 μm.

However, recent research on molecular-scale magnetic features has revealed astonishing results, such as the manipulaton of single molecular spins[19] or a new phase-separation mechanism in dispersions of nanorods,[20] which were not expected from established physical models.

To continue the line of research, we prove the opposite of what was stated above: we demonstrate that magnetic ions in a homogeneous aqueous solution can be locally enriched by means of a superimposed magnetic gradient field. Moreover, even the low gradient provided by a commercial NdFeB permanent magnet is sufficient for this, which is in strong contradiction with the established understanding. This finding is not only of high interest from the theoretical point of view but also of great importance for a variety of applications, either in terms of increasing sensor performances by local enrichment of the species to be detected or for recycling of, for example, rare-earth metals from industrial wastewater.

Paramagnetic $MnSO_4$ solutions with different concentrations, C_{MnSO_4}, were prepared using analytical grade reagents and deionized water. The total magnetic susceptibility of the solution is given by[16,21]

$$\chi_{sol} = \sum_k \chi_{mol,k} \cdot C_k \tag{2}$$

where $\chi_{mol,k}$ and C_k refer to the molar susceptibility of the molecules and concentration of sort k. Taking $\chi_{mol,H_2O} \cdot C_{H_2O} = -9 \times 10^{-6}$ into account along with the molar susceptibility of $MnSO_4$, $\chi_{mol,MnSO_4} = 1.716 \times 10^{-7}$ m^3/mol, we can derive the susceptibilities of the solutions used. In this way, we find, for example, 1.626×10^{-4} for a 1 M $MnSO_4$ solution.

A homogeneous $MnSO_4$ solution was injected into the cuboid glass cuvette with an inner side length of 10.0 mm. The cuvette was slightly overfilled to avoid any air bubbles and then sealed by means of a coverslip (glass thickness of 150 μm), which was moved over the top of the cell. We waited for 5 min to allow the flow associated with the filling to subside inside the cell. Then, a cylindrical NdFeB (neodymium−iron−boron) permanent magnet with a diameter of 10.0 mm and a height of 5.0 mm was placed 0.5 mm above the coverslip; see Figure 1a.

The resulting spatial distribution of the magnetic induction $\vec{B}$ around the magnet was simulated by means of a finite element solver (Amperes 9.0) and is axisymmetric by definition. Hence, the azimuthal component B_ϕ and the respective derivative $\partial/\partial\phi$ cancel out in the azimuthal direction. As a result, the following components in the r and z directions remain in the field gradient force density $\vec{f}_m$, eq 1

$$[(\vec{B}\cdot\nabla)\vec{B}]_r = B_r\frac{\partial B_r}{\partial r} + B_z\frac{\partial B_r}{\partial z} \tag{3}$$

$$[(\vec{B}\cdot\nabla)\vec{B}]_z = B_r\frac{\partial B_z}{\partial r} + B_z\frac{\partial B_z}{\partial z} \tag{4}$$

To intuitively understand the plots in Figure 1b−d, imagine the magnetic dipole, Figure 1a. The field lines exit at the magnet's north pole, which immediately faces the solution. Hence, in the upper central part of the solution, B_z is the dominating component (Figure 1b). By contrast, because of the bending of the field lines toward the opposite south pole, B_r becomes noticeable along the perimeter of the magnet, that is, at the upper sidewalls of the cuvette, see Figure 1c. Significant

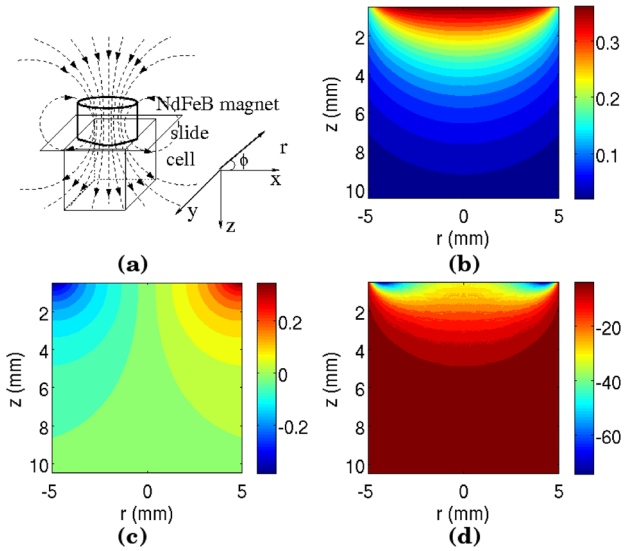

Figure 1. (a) Sketch of magnet and cell setup. (b,c) B_z and B_r in Tesla. (d) Dominant part, $B_z(\partial B_z/\partial z)$ in T^2/m, of the axial field gradient component according to eq 4.

gradients, $\partial B_r/\partial r$, appear only in the corners, whereas $\partial B_z/\partial z$ also penetrates the upper bulk solution. Thus, one can show that the dominant component in (eqs 3 and 4) is $B_z\partial B_z/\partial z$, as plotted in Figure 1d.

A Mach−Zehnder interferometer was used to study the evolving concentration distribution of $C_{Mn^{2+}}$ in the cell under the action of $\vec{f}_m$. It employs the fact that the refractive index, n, of the solution is a linear function of C_{MnSO_4} given by $n = 1.3339 + 0.0233(\text{mol/dm}^3)^{-1} \cdot C_{MnSO_4}$. The velocity distribution was measured using particle image velocimetry (PIV). The setup and details of both techniques were the same as those in our previous work.[22] The recording was carried out for 10 s at a time interval of 60 s for 20 to 30 min. The laser was blocked by a piece of dark paper during the recording off time to avoid any local heating of the cell. All results were time-averaged over 1 s, that is, 10 frames. Every measurement was conducted at room temperature for at least three times.

The key result of this work is the observation of a highly reproducible bending of the fringes in the interferograms directly below the magnet after the magnet is applied to the paramagnetic solution; see the Supporting Information. This clearly indicates a change in the refractive index Δn of the solution, which may be caused by a change in either the concentration or the temperature of the solution. However, no physical reason is identifiable for the latter because the solution was safely prevented from being heated by the laser or from cooling through evaporation. Therefore, we processed the interferogram packages under the assumption that Δn is entirely caused by a change in the concentration, $C_{Mn^{2+}}$, of the Mn^{2+} ions.

Figure 2 shows the resulting contour plots representing the change in $C_{Mn^{2+}}$ for three $MnSO_4$ solutions of different concentrations at t = 600 and 1200 s after the magnet was applied. For all solutions, we observed the formation of a convex layer close to the magnet in which $C_{Mn^{2+}}$ is higher than in the bulk. The enrichment at 1200 s is larger than that at 600 s and rises with the initial $MnSO_4$ concentration, C_0. The larger the amount of C_0, the stronger the concentration increase at the top, which is found to reach 2% of C_0.

dx.doi.org/10.1021/jz301561q | J. Phys. Chem. Lett. 2012, 3, 3559−3564

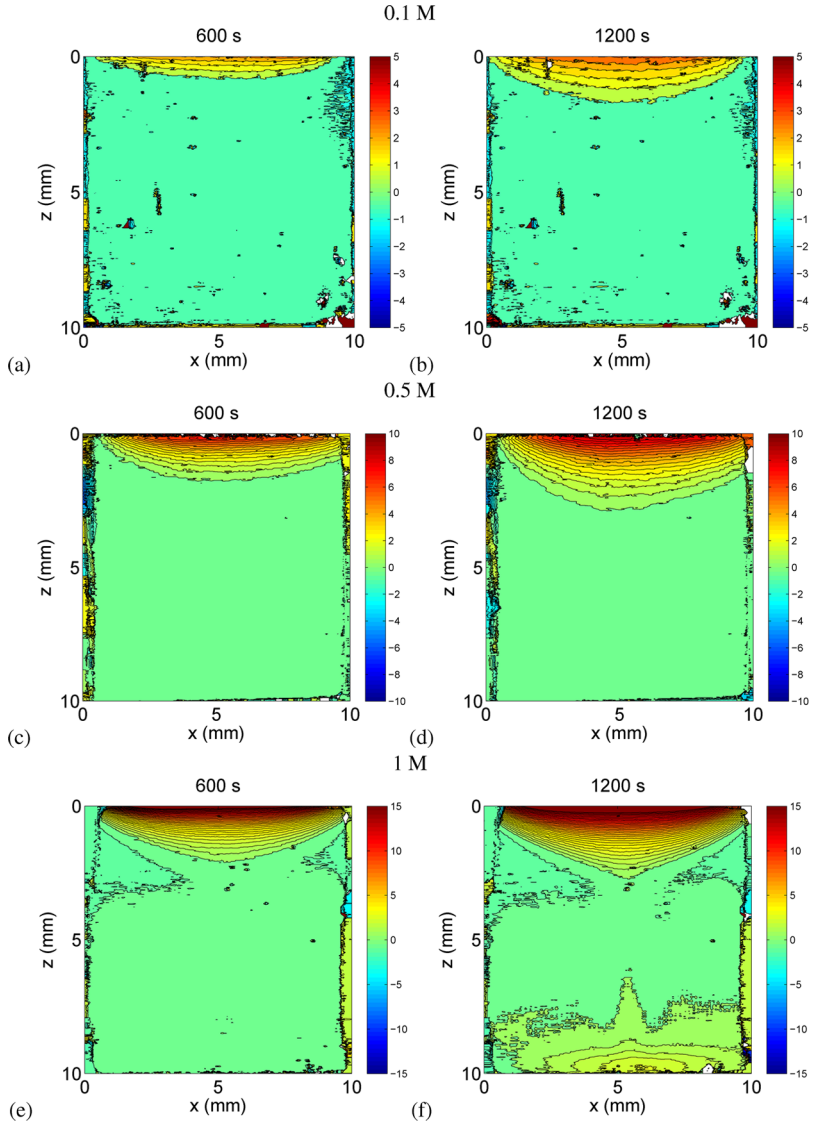

Figure 2. Iso-concentration contour plots of the $MnSO_4$ solution 600 (left column) and 1200 s (right column) after the magnet was applied on top of the cell. The unit in the legends is the concentration change in mM. The concentration of the initial solution was (a,b) 0.1, (c,d) 0.5, and (e,f) 1 M.

From the plots in Figure 2 we next extract the temporal evolution of the local concentration change along the center line (x = 5 mm) at different z positions in the cell (Figure 3a). The concentration change shows a clear height dependence, the smaller the distance to the magnet, the bigger the concentration increase. Even more importantly, the whole process can be divided into three different phases over time. In the first *induction* phase I, lasting from the application of the magnet at t = 0 s to about 100 s, no obvious concentration change occurs. In the second phase II, a continuous concentration increase occurs in the upper half of the cell until $t \approx 1000$ s; see Figure 3a. In parallel, a small decrease in the concentration at larger distance, for example, z = 2.0 mm, occurs in the interval (180−420) s. This can be attributed to the attraction of Mn^{2+} from this region toward the upper regions with a higher field gradient. Finally, in the third phase III, starting at $t \approx 1000$ s, the local concentrations run into a plateau with no further increase; that is, a steady state is established. Hence, $\vec{f}_m$ is obviously balanced by another force, buoyancy, as we will discuss later on.

To substantiate further the concentration enrichment, we plot the vertical concentration profile at different times after the magnet was applied in Figure 3b. We see that the concentration enrichment in the upper region (z < 2 mm) of the cell increases with time until about $t \approx 1000$ s, in line with Figure 3a. Interestingly, a concentration increase, although considerably smaller, also occurs at the bottom of the cell for $t \geq 600$ s.

The origin of this increase can be understood by zooming into the concentration contour plots and applying PIV in parallel. Figure 4a proves that there is a drainage from the enrichment layer down to the bottom center of the cell. This drainage, which feeds the increase at the bottom, is associated with a downward flow visualized by the PIV measurement in Figure 4b. The downward flow occurs in the center of the cell, that is, at the position of maximum bending of the concentration iso-contours in Figure 4a. Thus we can infer that the steady state in phase III results from a balance between an attraction of Mn^{2+} ions toward the magnet and their depletion due to a drainage by means of a downward flow.

dx.doi.org/10.1021/jz301561q | J. Phys. Chem. Lett. 2012, 3, 3559−3564

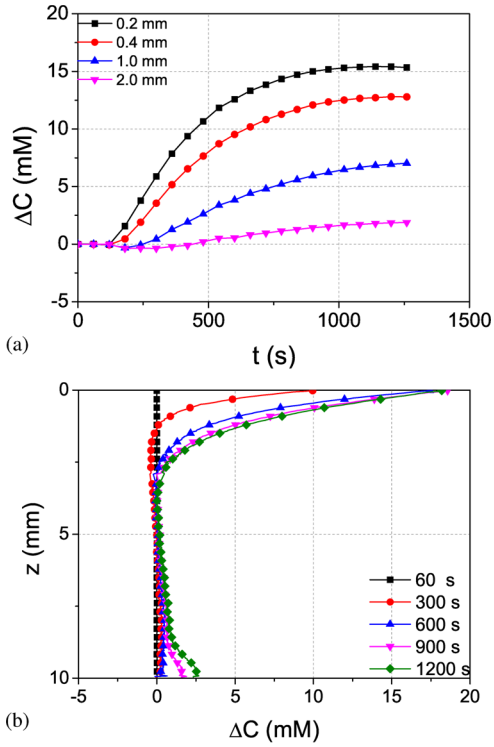

Figure 3. (a) Concentration change versus time at different distances z from the top (see legend) after the magnet was applied. (b) Vertical concentration profile in the z direction in the center of the cell (x = 5 mm) for different times after the magnet was applied. The bulk $MnSO_4$ concentration was 1 M.

The next important question to be answered is that of what happens when the magnet is removed in phase III. Figure 4 c,d shows that the enriched layer on top of the cell immediately drops down to the bottom in a few seconds. This closely resembles a Rayleigh−Taylor instability,[23] which occurs when a layer of higher density is imposed on another one of lower density. The falling plume, entraining the content of the enrichment layer, can be seen well in Figure 4c. This plume creates a downward flow in the center, which is clearly visible in the PIV, Figure 4d. By continuity, an upward flow occurs in the outer parts of the cell that replaces the fluid dragged from the enrichment layer.

The concentration enrichment that we report above is restricted neither to the paramagnetic Mn^{2+} ions nor to SO_4^{2-} as anions. We found that similar phenomena also occur for the stronger paramagnetic Gd^{3+} or for Cl^- as an anion. By contrast, no significant effect was found for the $CuSO_4$ solution because χ_{sol} and correspondingly $\vec{f}_m$ are much smaller than in $MnSO_4$.

The key observation is a demixing of paramagnetic solutions of manganese salts when they are brought into an inhomogenous magnetic field. To understand better the possible mechanism of this phenomenon, we first summarize its main features:

1. The convex shape of the optical inhomogeneous layer below the magnet reproduces the convex shape of the spatial distribution of the dominant component of the magnetic field gradient force (Figure 1d).
2. The temporal evolution proceeds in three phases, whereby the enrichment achieves saturation in phase III. Afterward, a central downward flow, visible using both PIV and interferometry, appears and drains the enriched liquid out of this layer.
3. The latter feature fits in with the fact that the enriched layer immediately falls down when the magnet is removed, proof that the enriched layer is heavier than the underlying solution.
4. The enrichment phenomenon is not restricted to $MnSO_4$ but is also observed both for other paramagnetic ions and for different anions.

This observed demixing of an initially homogeneous solution is a highly reproducible but unexpected phenomenon. Indeed, for the present case of a $MnSO_4$ solution in a closed system with concentrations significantly below the solubility product, one would not expect a demixing, even in the presence of the applied magnetic field. Therefore, we first speculated about a parasitic thermal effect. However, with the precautions explained above, both heating by the laser and evaporative cooling of the solution are excluded and hence also any kind of magnetocaloric pumping.[24] Also, no nanoparticle formation was detected using dynamic light scattering within 1 h of the solution being stored under experimental conditions. The lack of any indication of a thermal origin of the phenomenon thus motivated us to process the interferograms on the basis that the optical inhomogeneity detected results entirely from an inhomogeneous distribution of the paramagnetic Mn^{2+} species. In the following, we would like to show that this assumption appears reasonable.

To see which processes govern the distribution of Mn^{2+}, we start with the average magnetic moment per Mn^{2+} dipole (spin 1/2) in the distribution, which is given by[25]

$$<m> = g_L \mu_B \cdot \tanh\left(\frac{g_L \mu_B B}{kT}\right)\vec{B}/|\vec{B}| \tag{5}$$

g_L and μ_B refer to the Landé factor and Bohr's magneton, respectively. This allows us to calculate the magnetic energy per unit volume of the solution of concentration C according to $U_M^{volume} = -N_A C<m>\vec{B}$ with the Avogadro number $N_A = 6.022 \times 10^{23}$ mol^{-1}. Following the thermodynamic approach of Leventis and Gao[25] via the magneto-electrochemical potential of the manganese-ion species, the flux of Mn^{2+} with a diffusion coefficient D and velocity $\vec{v}$ is given by

$$\vec{N}_{Mn^{2+}} = -D\nabla C - \frac{2F}{N_A kT} CD\nabla\phi + 2DC\cdot\left(\frac{g_L \mu_B}{kT}\right)^2 (\vec{B}\cdot\nabla)\vec{B} + C\vec{v} \tag{6}$$

in which F is the Faraday number. Thus a Mn^{2+} flux in the solution may result from four effects, namely classical diffusion, migration in an electric field ($-\nabla\phi$), migration in a magnetic field gradient, and convection. In the present case, the second effect is not operating because $\nabla\phi$ vanishes.

Coming back to the experiment, we note that the third term in eq 6, migration, is small and should only be able to compete with diffusion at the beginning of the induction phase, where the concentration gradients are weak. Nevertheless, it appears that the second phase is governed by a migration in the magnetic field gradient, the counteracting diffusional term, and a possible convective effect. However, the latter lies below the resolution of our instrument because no visible drainage from the convex enrichment layer occurs in phase II, that is, $\vec{v} \approx 0$. This changes with the crossover to the third phase, Figures 2f

dx.doi.org/10.1021/jz301561q | J. Phys. Chem. Lett. 2012, 3, 3559−3564

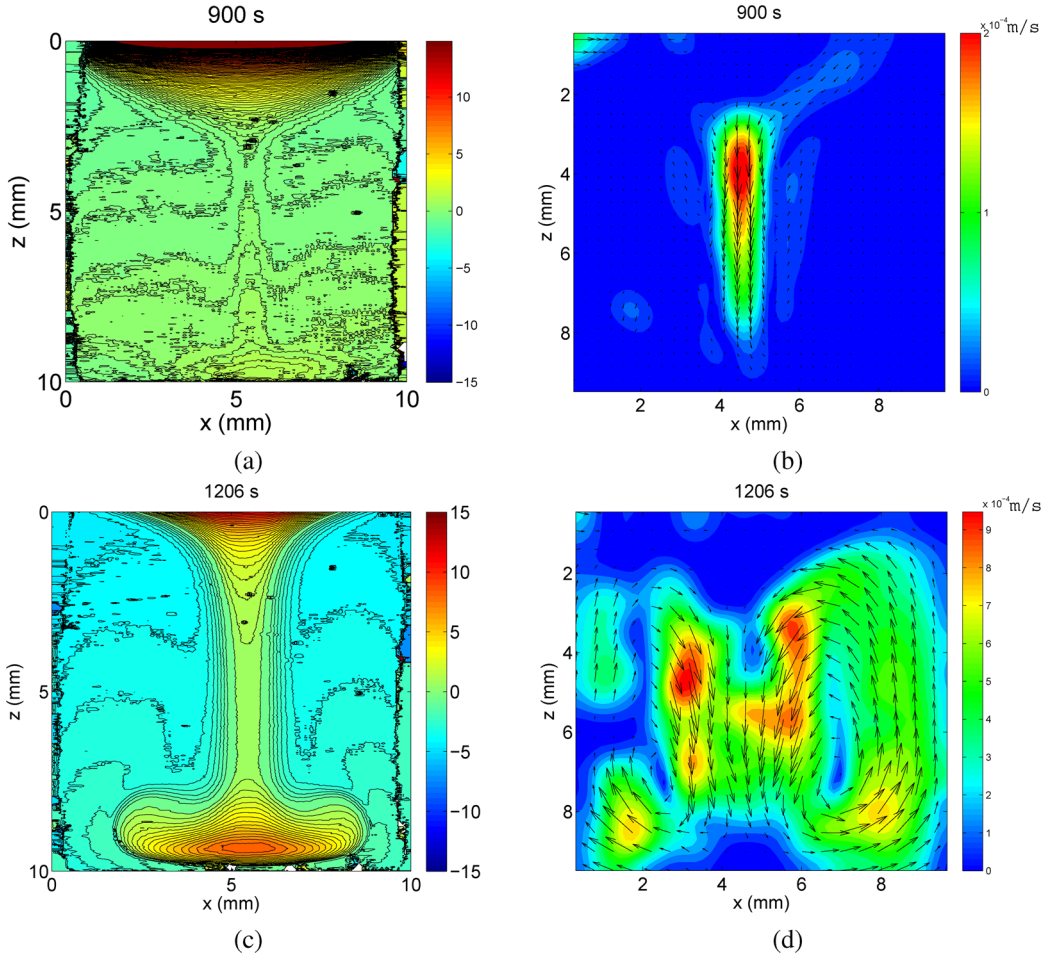

Figure 4. Iso-concentration contours (a,c) and velocity vector plots (b,d) 900 s after the magnet was applied on top of the cell (a,b) and 6 s after the magnet was removed (c,d) for the 1 M $MnSO_4$.

and 4a,b. The flow field $\vec{v}$, associated with the downflow, obeys the Navier–Stokes equation

$$\partial_t \vec{v} + \vec{v}\cdot\nabla\vec{v} = -\frac{1}{\rho_0}\nabla p + \nu\Delta\vec{v} + \frac{1}{\rho_0}\frac{\chi_{sol}}{\mu_0}(\vec{B}\cdot\nabla)\vec{B} + \frac{1}{\rho_0}\vec{f}_b \tag{7}$$

where ∇p is the pressure gradient and $\vec{f}_b = \rho_0\alpha(C_{Mn^{2+}} - C_0)\vec{g}$ is the buoyancy force density. Figure 4c,d proves that $\vec{f}_b$ must be present because the enrichment layer falls down upon removal of the magnet. Thus, an important quantity to be considered is the local increase in the density of the solution ρ [g cm^{-3}] with increasing $C_{Mn^{2+}}$ [M] due to the enrichment of Mn^{2+} according to

$$\rho = \rho_0(1 + \alpha[C_{Mn^{2+}} - C_0]) \tag{8}$$

with $\rho_0 = 1.13$ g cm^{-3} and a densification coefficient $\alpha = 0.1209 \times 10^{-3}$ m^3/mol for 1 M $MnSO_4$. Note that due to the convex shape of the enrichment layer, $\vec{f}_b$ immediately gives rise to a buoyancy-driven convection because $\nabla \times \vec{f}_b \neq 0$; see, for example, ref 26. The fact that we only see this flow after the crossover from phase II to phase III allows us to prove indirectly that the enrichment layer is an accumulation of paramagnetic Mn^{2+} ions. Indeed, because a steady state is attained in phase III, a balance between the attracting force density $\vec{f}_m$ and the counteracting $\vec{f}_b$ must exist such that $f_m \approx f_b$. Now quantifying the two forces, thereby going back to the natural Cartesian coordinate system of the cuboid cell, we find for the relevant z components[27]

$$f_m = \frac{\chi_{sol}}{2\mu_0}h\int\int dx\, dz\frac{\partial B^2_{(x,z)}}{\partial z},$$
$$f_b = \rho_0\alpha g h\int\int dx\, dz(C_{Mn^{2+}}(x,z) - C_0) \tag{9}$$

where $h = 0.01$m is the width of the cell in the y direction and g is the gravitational acceleration. Using $\chi_{sol} = 1.626 \times 10^{-4}$ and $\rho_0 = 1.13 \times 10^3$ kg/m^3 for 1 M $MnSO_4$ solution, we obtain the following values: $f_m = 0.8 \times 10^{-3}$ N and $f_b = 1.1 \times 10^{-3}$ N. The fact that the two forces, estimated on the basis of the material properties of $MnSO_4$, are of nearly identical magnitude strongly supports the assumption that enrichment of Mn^{2+} takes place locally, below the magnet.

We believe that this possibility to separate paramagnetic metal ions from aqueous solutions might open an avenue toward the recycling of permanent magnets, which are an important component in clean-energy technologies. To this end, further research is necessary to discover the mechanism by which the small magnetic migration term in eq 6 is able to stimulate such a pronounced enrichment. In this regard it is important to understand why there is no concentration change in the induction period or which sort of convective flow is associated with the enrichment of Mn^{2+}.

dx.doi.org/10.1021/jz301561q | J. Phys. Chem. Lett. 2012, 3, 3559–3564

■ ASSOCIATED CONTENT

Supporting Information

Detailed experimental setup, process of interferogram analysis, material properties, and animation showing the Rayleigh-Taylor instability of the enriched layer after removal of the magnet. This material is available free of charge via the Internet at http://pubs.acs.org.

■ AUTHOR INFORMATION

Corresponding Author

*E-mail: xuegeng.yang@tu-dresden.de (X.Y.); kerstin.eckert@tu-dresden.de (K.E.).

Notes

The authors declare no competing financial interest.

■ ACKNOWLEDGMENTS

We are grateful to our colleagues Gerd Mutschke and Tom Weier for many fruitful discussions. Financial support from Deutsche Forschungsgemeinschaft (DFG) in frame of the Collaborative Research Center (SFB) 609 is gratefully acknowledged.

■ REFERENCES

(1) Davidson, P. A. *An Introduction to Magnetohydrodynamics*; Cambridge University Press: New York, 2001.

(2) Weston, M. C.; Gerner, M. D.; Fritsch, I. Magnetic Fields for Fluid Motion. *Anal. Chem.* **2010**, *82*, 3411−3418.

(3) Nguyen, N. Micro-Magnetofluidics: Interactions between Magnetism and Fluid Flow on the Microscale. *Microfluid. Nanofluid.* **2010**, 1−16.

(4) Nikrityuk, P.; Eckert, K.; Grundmann, R. Contactless Mixing of Liquid Metals. *Metall. Mater. Trans. B* **2010**, *41*, 94−111.

(5) Willers, B.; Eckert, S.; Nikrityuk, P.; Räbiger, D.; Dong, J.; Eckert, K.; Gerbeth, G. Efficient Melt Stirring Using Pulse Sequences of a Rotating Magnetic Field: Part II. Application to Solidification of Al-Si Alloys. *Metall. Mater. Trans. B* **2008**, *39*, 304−316.

(6) Koza, J. A.; Uhlemann, M.; Gebert, A.; Schultz, L. The Effect of Magnetic Fields on the Electrodeposition of CoFe Alloys. *Electrochim. Acta* **2008**, *53*, 5344−5353.

(7) Qian, S.; Bau, H. Magneto-Hydrodynamics Based Microfluidics. *Mech. Res. Commun.* **2009**, *36*, 10−21.

(8) Weston, M.; Nash, C.; Fritsch, I. Redox-Magnetohydrodynamic Microfluidics without Channels and Compatible with Electrochemical Detection under Immunoassay Conditions. *Anal. Chem.* **2010**, *82*, 7068−7072.

(9) Doyle, P.; Bibette, J.; Bancaud, A.; Viovy, J. Self-Assembled Magnetic Matrices for DNA Separation Chips. *Science* **2002**, *295*, 2237−2237.

(10) Pamme, N. Magnetism and Microfluidics. *Lab Chip* **2006**, *6*, 24−38.

(11) Zhang, K.; Liang, Q.; Ma, S.; Mu, X.; Hu, P.; Wang, Y.; Luo, G. On-Chip Manipulation of Continuous Picoliter-Volume Superparamagnetic Droplets Using a Magnetic Force. *Lab Chip* **2009**, *9*, 2992−2999.

(12) Suwa, M.; Watarai, H. Magnetoanalysis of Micro/nanoparticles: a Review. *Anal. Chim. Acta* **2011**, *690*, 137−147.

(13) Lim, J.; Lanni, C.; Evarts, E.; Lanni, F.; Tilton, R.; Majetich, S. Magnetophoresis of Nanoparticles. *ACS Nano* **2010**, *5*, 217−226.

(14) Rosensweig, R. *Ferrohydrodynamics*; Dover Publications: Mineola, NY, 1997.

(15) Tschulik, K.; Cierpka, C.; Gebert, A.; Schultz, L.; Kaehler, C. J.; Uhlemann, M. In Situ Analysis of Three-Dimensional Electrolyte Convection Evolving during the Electrodeposition of Copper in Magnetic Gradient Fields. *Anal. Chem.* **2011**, *83*, 3275−3281.

(16) Coey, J. M. D.; Aogaki, R.; Byrne, F.; Stamenov, P. Magnetic Stabilization and Vorticity in Submillimeter Paramagnetic Liquid Tubes. *Proc. Natl. Acad. Sci. U. S. A.* **2009**, *106*, 8811−8817.

(17) Chie, K.; Fujiwara, M.; Fujiwara, Y.; Tanimoto, Y. Magnetic Separation of Metal Ions. *J. Phys. Chem. B* **2003**, *107*, 14374−14377.

(18) Fujiwara, M.; Chie, K.; Sawai, J.; Shimizu, D.; Tanimoto, Y. On the Movement of Paramagnetic Ions in an Inhomogeneous Magnetic Field. *J. Phys. Chem. B* **2004**, *108*, 3531−3534.

(19) Miguel, J.; Hermanns, C. F.; Bernien, M.; Krueger, A.; Kuch, W. Reversible Manipulation of the Magnetic Coupling of Single Molecular Spins in Fe-Porphyrins to a Ferromagnetic Substrate. *J. Phys. Chem. Lett.* **2011**, *2*, 1455−1459.

(20) van den Pol, E.; Lupascu, A.; Diaconeasa, M. A.; Petukhov, A. V.; Byelov, D. V.; Vroege, G. J. Onsager Revisited: Magnetic Field Induced Nematic-Nematic Phase Separation in Dispersions of Goethite Nanorods. *J. Phys. Chem. Lett.* **2010**, *1*, 2174−2178.

(21) Tschulik, K.; Yang, X.; Mutschke, G.; Uhlemann, M.; Eckert, K.; Sueptitz, R.; Schultz, L.; Gebert, A. How to Obtain Structured Metal Deposits from Diamagnetic Ions in Magnetic Gradient Fields? *Electrochem. Commun.* **2011**, 13,946−950.

(22) Yang, X.; Eckert, K.; Muehlenhoff, S.; Odenbach, S. On the Decay of the Lorentz-Force-Driven Convection in Vertical Concentration Stratification during Magnetoelectrolysis. *Electrochim. Acta* **2009**, *54*, 7056−7065.

(23) Fernandez, J.; Kurowski, P.; Petitjeans, P.; Meiburg, E. Density-Driven Unstable Flows of Miscible Fluids in a Hele-Shaw Cell. *J. Fluid Mech.* **2002**, *451*, 239−260.

(24) Love, L.; Jansen, J.; McKnight, T.; Roh, Y.; Phelps, T. A Magnetocaloric Pump for Microfluidic Applications. *IEEE Trans. Nanobiosci.* **2004**, *3*, 101−110.

(25) Leventis, N.; Gao, X. Magnetohydrodynamic Electrochemistry in the Field of Nd-Fe-B Magnets. Theory, Experiment, and Application in Self-Powered Flow Delivery Systems. *Anal. Chem.* **2001**, *73*, 3981−3992.

(26) Mutschke, G.; Bund, A. On the 3D Character of the Magnetohydrodynamic Effect During Metal Electrodeposition in Cuboid Cells. *Electrochem. Commun.* **2008**, *10*, 597−601.

(27) Mutschke, G.; Tschulik, K.; Weier, T.; Uhlemann, M.; Bund, A.; Froehlich, J. On the Action of Magnetic Gradient Forces in Micro-Structured Copper Deposition. *Electrochim. Acta* **2010**, *55*, 9060−9066.